JOURNAL OF MATERIALS SCIENCE **38** (2003) 4393–4405

Multiscale modeling of particle-modified polyethylene

J. A. W. VAN DOMMELEN, W. A. M. BREKELMANS, F. P. T. BAAIJENS
Dutch Polymer Institute, Eindhoven University of Technology, Department of Mechanical Engineering, P.O. Box 513, 5600 MB Eindhoven, The Netherlands
E-mail: J.A.W.v.Dommelen@tue.nl

A common practice in toughening of semicrystalline polymers is to blend them with second-phase rubber particles. A toughening mechanism has recently been suggested which considers a layer of transcrystallized material around well-dispersed particles. This layer has a reduced yield strength in certain preferentially oriented directions. A multiscale numerical model is used to investigate the effect of such a specific microstructural morphology on the mechanical behavior of voided systems. A polycrystalline model is used for high density polyethylene (HDPE) matrix material. The basic structural element in this model is a layered two-phase composite inclusion, comprising both a crystalline and an amorphous domain. The averaged fields of an aggregate of composite inclusions, having either a random or a preferential orientation, form the constitutive behavior of the polymeric matrix material. The anisotropy of material with preferential orientations is determined. The particle-dispersed system is described by finite element RVE models, with in each integration point an aggregate of composite inclusions. Transcrystallized orientations are found to have a limited effect on matrix shear yielding and alter the triaxial stress field. An hypothesized, flow-influenced, microstructure is shown to further improve material properties if loaded in the appropriate direction.

1. Introduction

The application of semicrystalline polymeric materials is often limited by some unfavorable mechanical properties, such as their often occurring brittle response. An empirical procedure for toughening of these material is to blend them with second-phase rubber particles. The present-day notion of the toughening mechanism in these materials is based on the criterion proposed by Wu [1], which states that a sharp brittle/tough transition occurs for nylon/rubber blends when the average interparticle matrix ligament thickness Λ is reduced below a critical value Λ_c, as is schematically shown in Fig. 1. Wu considered this transition to be a consequence of the mutual interaction of particle disturbed stress fields, which enhances matrix yielding. Borggreve *et al.* [2] confirmed the existence of a critical interparticle distance for the brittle/tough transition, but questioned the physical explanation by Wu. Thereafter, a modified theory was proposed, in which the critical ligament thickness corresponds to a local plane strain to plane stress transition in the matrix [3, 4]. Based on their numerical investigations, Fukui *et al.* [5] and Dijkstra and Ten Bolscher [6] attributed the toughening effect to extensive shear yielding due to the interaction of stress fields. However, since these stress field theory results are affected by changes in geometrical ratios, it can be concluded that they are inadequate in explaining the existence of an absolute length scale such as a critical interparticle distance.

A physical basis of the absolute length parameter was offered by Muratoğlu *et al*. [7, 8], who recognized the brittle/tough transition as a true material feature, which is attributed to thin layers of preferentially oriented material, with a reduced plastic resistance, appearing in the microstructural morphology of particle-modified semicrystalline material. Accordingly, the crystallization behavior of the matrix is influenced by the rubber/matrix interface, leading to a layer of parallel crystalline lamellae, nucleated at the interface, with the crystalline planes having the lowest plastic resistance co-directional with the interface. It was experimentally established that these transcrystalline layers have a well-defined thickness of approximately $\Lambda_c/2$. When the average matrix ligament thickness Λ is below the critical value Λ_c, the favorably oriented material percolates through the system, bridging between the second-phase particles, as is shown in Fig. 2b. Additionally, the situation with $\Lambda \gg \Lambda_c$ is represented in Fig. 2a. A blended system consists of (i) rubber particles having a low modulus, (ii) preferentially oriented anisotropic matrix material enveloping the particles and (iii) the bulk matrix material having a randomly oriented structure and effectively having isotropic material properties. According to the toughening mechanism postulated by Muratoğlu *et al.* [8], after cavitation of the

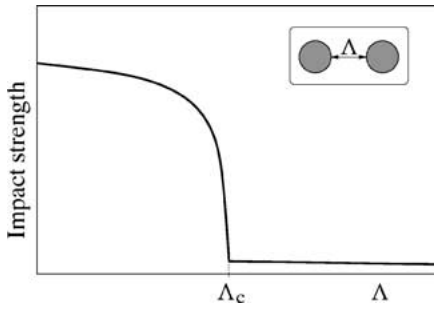

Figure 1 Impact toughness of nylon/rubber blends vs. the average surface–to–surface interparticle ligament thickness Λ. Adopted from Wu [1].

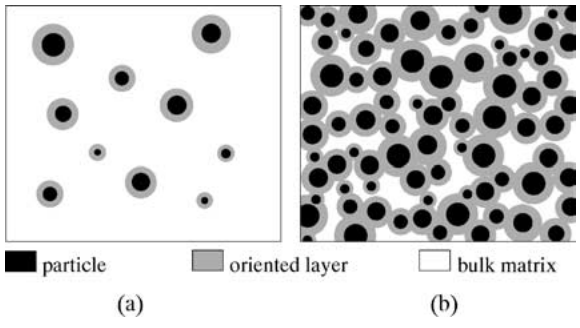

Figure 2 Transcrystallized layers around second-phase particles for (a) $\Lambda \gg \Lambda_c$, with a brittle response and for (b) $\Lambda \leq \Lambda_c$ where the material with a decreased plastic resistance percolates through the blend, enhancing the toughness. Adopted from [8] and [10].

second-phase rubber particles, the regions with a lowered yield resistance will facilitate large plastic deformation and thereby improve toughness. Tzika *et al.* [9] used a micromechanical numerical model, with a staggered array of particles, to study the influence of preferentially oriented anisotropic layers, modeled with anisotropic Hill plasticity, on the deformation mechanisms under high triaxiality conditions. They observed plastic deformation in the matrix to occur diagonally away from particles (i.e., in the matrix material between particles, parallel to the interfaces) for $\Lambda \leq \Lambda_c$, rather than bridging between particles surfaces for $\Lambda \gg \Lambda_c$.

Bartczak *et al.* [10, 11] generalized the Wu criterion to other materials (such as HDPE) and showed the critical interparticle distance to be an intrinsic property of the matrix material, thereby opening the possibility of using mineral fillers for the toughening of semicrystalline polymers, the advantage of which would be an improved modulus of the blend. They argued that debonding of hard filler particles could be an alternative for the cavitation of the rubbery phase. However, the Bartczak *et al.* results showed a distinct effect of processing conditions on the obtained toughness. The importance of process conditions was demonstrated by Schrauwen *et al.* [12], who found toughness to be dominated by flow-induced effects.

In Van Dommelen *et al.* [13], idealized polymeric matrix material was modeled by anisotropic Hill plasticity, and various representative volume elements were used to describe the system containing dispersed voids. It was shown that local plastic anisotropy of matrix material around the voids can very effectively replace localization by dispersed shear yielding and change the occurring hydrostatic stresses, potentially leading to toughened material behavior. However, to achieve these improvements, a morphology must be pursued that (i) has a radially oriented structure around the dispersed particles, and (ii) provides a sufficiently large amount of anisotropy. Moreover, in Van Dommelen *et al*. [14], the efficiency of this mechanism is found to be affected by the presence of hard filler particles.

To investigate the possibility that a particular microstructure satisfies the above-mentioned requirements, a micromechanically-based numerical model for the elasto-plastic deformation and texture evolution of semicrystalline polymers [15] has been developed and will be used to simulate the behavior of particle-modified polyethylene. For the analysis of these systems, a distinction between three different scales is made, as schematically depicted in Fig. 3. The constitutive properties of the material components are characterized at the microscopic scale. At this scale, the individual crystallographic lamellae and amorphous layers are identified and modeled as elasto-viscoplastic. The crystalline lamellae are assumed to deform plastically by crystallographic slip, whereas plastic flow of the amorphous phase is modeled as a rate-dependent process with strain hardening resulting from molecular

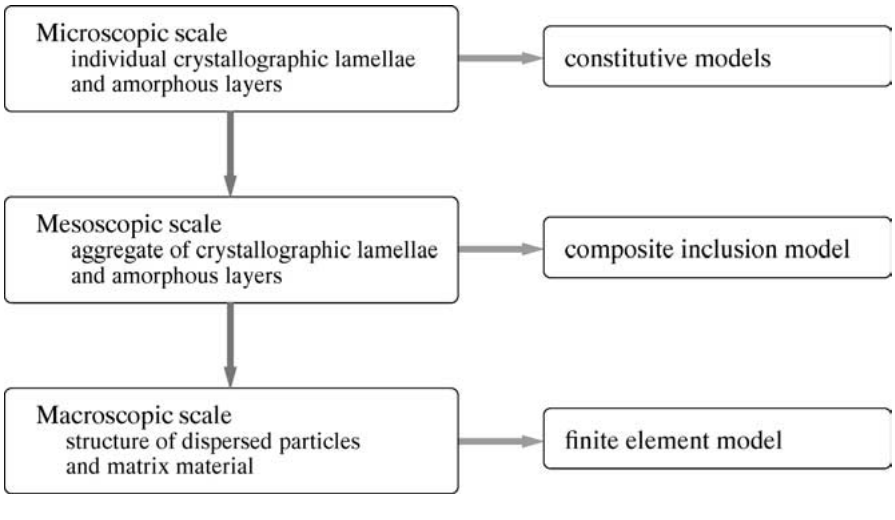

Figure 3 Different scales which can be identified in the analysis of particle-toughened semicrystalline polymeric systems.

orientation. At the mesoscopic scale, an aggregate of individual phases is formed, which can be a spherulite or a sheaflike aggregate of preferentially oriented material. To bridge between those scales, a composite inclusion model is adopted from Van Dommelen *et al.* [15]. The microscopic deformation and stress fields are related to the mesoscopic fields of the aggregate by a hybrid interaction law. At the macroscopic scale, for particle-modified materials, a structure of dispersed particles and matrix material can be identified. At this level, the system is represented by a finite element model using various representative volume elements, as suggested by Hill-type simulations [13]. A bridge to the mesoscopic level is formed by using an aggregate of composite inclusions as a representative microstructural unit in each integration point. The effect of a transcrystallized orientation of matrix material versus randomly oriented material on both mesoscopic and microscopic results is investigated. A limited shear yielding effect of transcrystallized orientation is observed. Additionally, further improved properties are obtained for a hypothesized microstructure (which may be the result of process conditions) if loaded in the appropriate direction.

2. Microscopic scale: material models

The constitutive behavior of semicrystalline polymeric material is modeled by an aggregate of two-phase composite inclusions. Each inclusion consists of a crystalline and an amorphous phase. In this section, the constitutive models of the composing phases are shortly discussed. For a more elaborate presentation of these models, see Van Dommelen *et al.* [15].

2.1. Crystalline phase

The crystalline domain of polymeric material consists of regularly ordered molecular chains. The crystal structure results in (i) anisotropic elastic behavior, and (ii) plastic deformation governed primarily by crystallographic slip on a limited number of slip planes [16, 17].

The elastic component of the deformation in the crystalline phase is characterized by an anisotropic fourth-order elastic modulus tensor which linearly relates the elastic Green–Lagrange strain tensor and an elastic second Piola–Kirchhofflike stress measure. The anisotropic elastic properties are coupled to the crystallographic directions. For the viscoplastic behavior of the crystalline phase, a rate-dependent crystal plasticity model is used. In this model, the plastic velocity gradient of the crystalline lamella, consisting of a single crystal, is composed of the contributions of all physically distinct slip systems. The shear rate of each slip system is assumed to be related to the resolved shear stress via a viscoplastic power law relation.

2.2. Amorphous phase

The amorphous domain of semicrystalline polymeric material consists of an assembly of disordered macromolecules, which are morphologically constrained by the neighboring crystalline lamellae. Plastic deformation in these domains occurs by the thermally activated rotation of segments. At room temperature, the amorphous phase of HDPE, which is the material of interest in this work, is in the rubbery regime, with the glass transition temperature near -70°C. The deformation is characterized by a limited strain rate sensitivity and a strong entropic hardening at large deformations.

The initial elastic resistance of the rubbery amorphous phase is well below the elastic resistance of the crystalline domain. Consequently, elastic deformations can be considerably large and are modeled by a generalized neo-Hookean relationship. A relatively strain rate insensitive viscoplastic power law relation between an effective shear strain rate and the effective shear stress [18] is adopted in conjunction with a back stress tensor for which the Arruda–Boyce eight-chain network model of rubber elasticity [19] is used.

3. Mesoscopic scale: composite inclusion model

When slowly cooled from the melt, many polymers, such as for example polyethylene, possess a polycrystalline structure with often a spherulitic morphology, e.g. [16, 20, 21]. Each spherulite consists of a radial assembly of thin crystalline lamellae which are separated by amorphous layers. Furthermore, in thin films crystallized on a substrate, a sheaflike morphology with preferentially-oriented crystalline lamellae is observed, e.g. [22].

The mechanical behavior at the mesoscopic level is modeled by an aggregate of layered two-phase composite inclusions [18, 23]. Each separate composite consists of a crystalline lamella which is mechanically coupled to its associated amorphous layer. The stress and deformation fields within each phase are assumed to be piecewise homogeneous, however, they may differ between the two coupled phases. It is assumed that the crystalline and the amorphous components remain fully mechanically coupled. Both kinematic compatibility within the composite inclusion and traction continuity across the interface are enforced. To relate the volume-averaged mechanical behavior of each composite inclusion to the imposed boundary conditions for an aggregate of inclusions, a hybrid local–global interaction law is used. This class of hybrid-inclusion models was introduced by Lee *et al.* [18, 23] for rigid/viscoplastic composite inclusions.

A more detailed description of the composite inclusion model is presented elsewhere [15]. Some aspects of the implementation of this model in the finite element package ABAQUS [24] are given in Van Dommelen *et al.* [25].

4. Anisotropy of preferentially oriented material

In the next sections, a full multiscale model will be used to investigate the effect of the microstructural morphology on the mechanics of particle-modified systems. First, in this section, the anisotropy, at the mesoscopic level, of (microscopically) preferentially oriented material, as predicted by the composite inclusion model,

is investigated. An aggregate of composite inclusions, represented by a set of crystallographic orientations and corresponding lamellar orientations, will be subjected to constant strain rate uniaxial tension in one of the three principal directions $\boldsymbol{e}_i$ of the material coordinate system:

$$\bar{\boldsymbol{R}} = \boldsymbol{I}; \quad \bar{U}_{ii} = \lambda(t); \quad i = 1 \vee i = 2 \vee i = 3, \quad (1)$$

with

$$\lambda(t) = \exp(\dot{\varepsilon} t), \quad (2)$$

where $\dot{\varepsilon}$ is set equal to the material reference shear rate $\dot{\gamma}_0$, $\bar{\boldsymbol{R}}$ is the mesoscopic rotation tensor, and $\bar{\boldsymbol{U}}$ is the corresponding right stretch tensor. Furthermore, the components of the mesoscopic Cauchy stress tensor $\bar{\boldsymbol{\sigma}}$ should satisfy:

$$\bar{\sigma}_{jj} = \bar{\sigma}_{12} = \bar{\sigma}_{13} = \bar{\sigma}_{23} = 0; \quad j \in \{1, 2, 3 \mid j \neq i\}. \quad (3)$$

In another test case, pure shear deformation is applied by prescribing one of the basic shear components ij of the (symmetric) right stretch tensor:

$$\bar{\boldsymbol{R}} = \boldsymbol{I}; \quad \bar{U}_{ij} = \gamma(t); \quad ij = 12 \vee ij = 13 \vee ij = 23, \quad (4)$$

with

$$\gamma(t) = \frac{1}{2}\sqrt{3}\dot{\gamma}_0 t, \quad (5)$$

and

$$\bar{\sigma}_{11} = \bar{\sigma}_{22} = \bar{\sigma}_{33} = \bar{\sigma}_{kl} = 0; \quad kl \in \{12, 13, 23 \mid kl \neq ij\}. \quad (6)$$

4.1. Randomly oriented material

The local spherulitic structure of melt-crystallized HDPE is represented by an aggregate of 125 composite inclusions with randomly generated initial orientations of the crystallographic phases, having an orthorhombic lattice. The distribution of orientations of the principal lattice directions is represented in Fig. 4a–c. Experimental studies of melt-crystallized polyethylene show that the lamellar surfaces are of the $\{h0l\}$-type, where the angle between the chain direction c and the lamellar normal n^{I} varies between 20° and 40° [26, 20]. Gautam *et al.* [27] have found, by molecular simulations, the {201} planes, having a chain/normal tilt angle of 35°, to provide the lowest crystal/amorphous interface energy. Here, the initial angle between c_0 and n_0^{I} is set at 35°, corresponding to the {201} planes. The initial orientations of the lamellar normals are shown in Fig. 4d. Since the distribution of the crystallographic orientations is random, the mechanical behavior of this aggregate will be quasi isotropic. The material properties at the microscopic level are adopted from Van Dommelen *et al.* [15]. The aggregate is subjected to the boundary conditions previously described; the obtained equivalent mesoscopic stress $\bar{\sigma}^{\mathrm{eq}} = \sqrt{\frac{3}{2}\bar{\boldsymbol{\sigma}}^{\mathrm{d}} : \bar{\boldsymbol{\sigma}}^{\mathrm{d}}}$, with $\bar{\boldsymbol{\sigma}}^{\mathrm{d}} = \bar{\boldsymbol{\sigma}} + \bar{p}\boldsymbol{I}$ the mesoscopic deviatoric stress tensor and $\bar{p} = -\frac{1}{3}\mathrm{tr}(\bar{\boldsymbol{\sigma}})$ the mesoscopic hydrostatic pressure, as a function of the imposed deformation, is represented in Fig. 4e. The equivalent stresses are normalized by the lowest slip resistance $\tau_0 = 8$ MPa. The number of inclusions within an aggregate should be sufficiently large, in order to expel the influence of the particular set of initial inclusions, and to mimic a truly isotropic material behavior. Here, the number of inclusions that comprise an aggregate is limited to 125, hence a quasi isotropic response is obtained. The influence of the aggregate size on the mesoscopic behavior was demonstrated in Van Dommelen *et al.* [25].

4.2. Transcrystallized material

The criterion for toughness of semicrystalline polymers, which was initially proposed by Muratoğlu *et al.* [8] for nylon/rubber blends and was extended to HDPE with rubber or calcium carbonate fillers by Bartczak

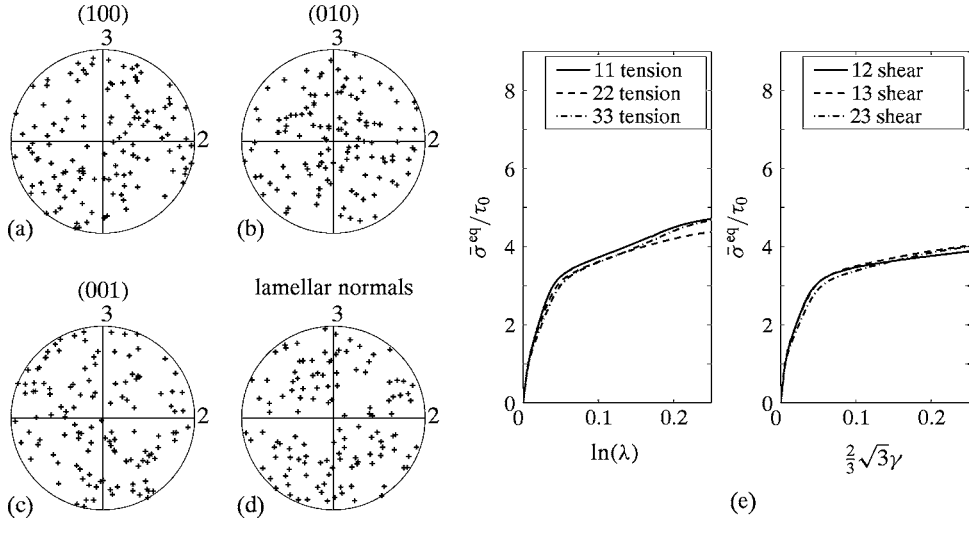

Figure 4 Equal area projection pole figures representing (a)–(c) the principal crystallographic lattice directions, and (d) the lamellar normals of a random set of orientations and (e) the normalized equivalent mesoscopic stress $\bar{\sigma}^{\mathrm{eq}}/\tau_0$, vs. the imposed deformation for tension and shear in the basic material directions as predicted by the composite inclusion model.

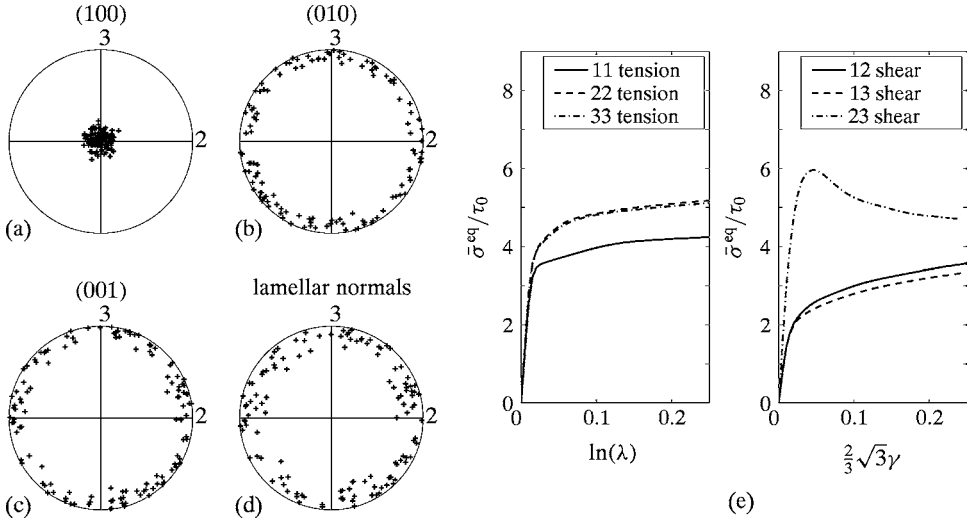

Figure 5 Equal area projection pole figures representing (a)–(c) the principal crystallographic lattice directions, and (d) the lamellar normals of a set of transcrystallized orientations and (e) the normalized equivalent mesoscopic stress $\bar{\sigma}^{eq}/\tau_0$, vs. the imposed deformation for tension and shear in the material base directions as predicted by the composite inclusion model.

et al. [10, 11], is based on transcrystallized matrix material around well dispersed particles. A similar morphology, namely unidirectionally grown crystalline lamellae, was found in polymeric material crystallized on planar substrates [7, 22]. For thin HDPE films, crystallized on rubber and calcium carbonate substrates, Bartczak *et al.* [22] found a sheaflike morphology of the lamellae, which were oriented preferentially edge-on against the substrate, resulting from a surface-induced crystallization. The (100) planes, containing the two crystallographic slip systems with the lowest slip resistance, (100)[001] and (100)[010], were found to be directed preferentially parallel to the plane of the film with a random orientation of the molecular chains within this plane. The lamellar normals were either parallel to the plane of the substrate or somewhat tilted with respect to the plane.

However, twisting of lamellae was found to be substantially reduced. The preferred crystallographic planes for the crystal/amorphous interface remain unclear for this morphology. It can be assumed that these planes are still of the $\{h0l\}$-type. The observation by Bartczak *et al.* [22] that crystal growth is unidirectional with little divergence sideways, and the reduction of lamellar twisting, suggest a smaller angle between the crystallographic chain direction c and the lamellar normal n^{I} than observed in randomly crystallized material. Here, the plane of the crystal/amorphous interface is assumed to be of the {102}-type, corresponding to an initial tilt angle of 9.7°. Besides the crystallographic and lamellar orientations, all microscopic material properties are assumed to be identical to the properties of the randomly crystallized material. A set of crystallographic orientations is generated with the (100) poles preferentially aligned in the direction of the normal of the substrate, with a certain random deviation from the substrate normal direction. Furthermore, a random rotation around this normal direction is applied. Therefore, the mechanical properties at the mesoscopic scale can be expected to be transversely isotropic with the (fiber) symmetry direction corresponding to the substrate normal direction. All differences in mechanical response in the 22 and 33 tensile directions and the 12 and 13 shear directions will be of statistical origin. After a set of crystallographic orientations has been generated, the lamellar normals are obtained as described above. In Fig. 5a–d, the orientations of a set of 125 composite inclusions are displayed. The view direction of the equal area pole figures is the substrate normal direction. This direction is the preferred direction for the (100) poles. In Fig. 5e, the corresponding mesoscopic stress–strain response of the composite inclusion model is shown in the basic tensile and shear directions. With respect to the randomly oriented aggregate, the equivalent stresses in the transverse tensile directions are increased. The reduction of the 12 and 13 shear resistances is related to these tensile 22 and 33 resistances. The ratio of transverse tensile and 12/13 shear resistances at the onset of yielding is of the order of 2. At higher strains, this ratio decreases to the order of 1.5. Simulations with an anisotropic Hill plasticity model [13] showed that for the toughening mechanism under investigation to be effective, a larger amount of anisotropy would be necessary. A sharper texture, however, does not increase the R_{22}/R_{12} anisotropy ratio.

5. Macroscopic scale: representative volume elements

For particle-toughened materials, a structure of dispersed particles and matrix material can be identified. The system is described by a finite element model of a representative volume element (RVE). The particle-modified system, having a three-dimensional nature, is simplified to a two-dimensional RVE, for which two different approaches are used. In order to capture the important effects of the essentially irregular nature of a system of dispersed particles, a multiparticle plane strain RVE [28] is used. For a representation of the triaxial stress state around a particle, an axisymmetric RVE, with a regular particle arrangement, is used, as suggested by Socrate and Boyce [29] and Tzika *et al.*

[9]. A comparison with fully three-dimensional calculations is presented elsewhere [13] for idealized polymeric material.

5.1. Multiparticle plane strain RVE

To account for the irregular nature of particle-dispersed systems, a plane strain RVE with irregularly dispersed particles (referred to as the *ID model*) is used, where the cavitated particles are represented by voids. In Fig. 6a, a schematic illustration of this RVE is shown. The periodicity assumption requires full compatibility of each opposite boundary pair. The corresponding essential and natural boundary tyings [30] for related points on opposite boundaries are given by:

$$\boldsymbol{u}|_{\Gamma_{34}} - \boldsymbol{u}|_{C_4} = \boldsymbol{u}|_{\Gamma_{12}} - \boldsymbol{u}|_{C_1}; \tag{7}$$

$$\boldsymbol{u}|_{\Gamma_{14}} - \boldsymbol{u}|_{C_1} = \boldsymbol{u}|_{\Gamma_{23}} - \boldsymbol{u}|_{C_2}; \tag{8}$$

$$\boldsymbol{\sigma}\cdot\boldsymbol{n}|_{\Gamma_{12}} = -\boldsymbol{\sigma}\cdot\boldsymbol{n}|_{\Gamma_{34}}; \tag{9}$$

$$\boldsymbol{\sigma}\cdot\boldsymbol{n}|_{\Gamma_{14}} = -\boldsymbol{\sigma}\cdot\boldsymbol{n}|_{\Gamma_{23}}, \tag{10}$$

where $\boldsymbol{n}$ denotes the outward unit normal of the boundary in the actual state. A tensile loading condition is prescribed on vertex C_2, and is given by

$$u_x|_{C_2} - u_x|_{C_1} = L_0[\exp(\dot{\varepsilon}t) - 1], \tag{11}$$

where $\dot{\varepsilon}$ is set equal to the reference strain rate, $\dot{\gamma}_0 = 10^{-3}\ \mathrm{s}^{-1}$, of the material. Furthermore, rotations are prevented by the following condition for the vertices C_1 and C_2:

$$u_y|_{C_1} = u_y|_{C_2}. \tag{12}$$

The displacements of C_4 are unspecified, whereas the displacements of C_3 are tied to the other vertices.

A structure with 20 volume percent irregularly dispersed voids is generated using a procedure from Hall [31] and Smit *et al.* [28]. In order to obtain initially straight boundaries, no void is allowed to cross a boundary. The mesh with 565 4-noded bilinear reduced integration plane strain elements is shown in Fig. 6b. An orientation field is generated by taking the local 1-directions perpendicular to the closest void/matrix interface, taking into account the periodicity of the structure, and is shown in Fig. 6c.

5.2. Axisymmetric RVE

An axisymmetric RVE model of a staggered array of particles (referred to as the *SA model*) is considered, which was previously used for the study of the micromechanics of particle-modified polymers by Socrate and Boyce [29] and by Tzika *et al.* [9] and which corresponds to a body centered tetragonal stacking of particles. A schematic representation of the RVE, with $L_0 = R_0$, is shown in Fig. 7a and b, where the cavitated particle is represented as a void. The RVE is subjected to anti-symmetry conditions (with respect to point M) along the outer radius, which were introduced by Tvergaard [32, 33]. Axial compatibility along the radial boundary Γ_{34} is written as

$$u_z(z_0|_M - \eta) + u_z(z_0|_M + \eta) = 2u_z|_M. \tag{13}$$

The combined cross-sectional area of neighboring cells is assumed to remain constant along the axial

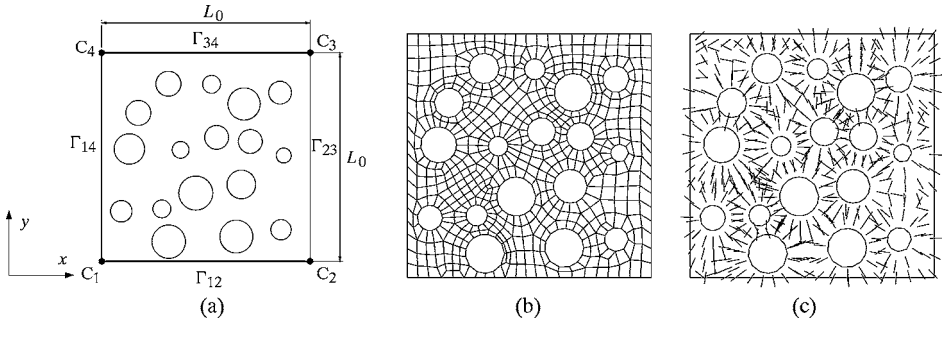

Figure 6 (a) Schematic visualization of an irregular plane strain RVE, (b) finite element mesh, and (c) local material orientations.

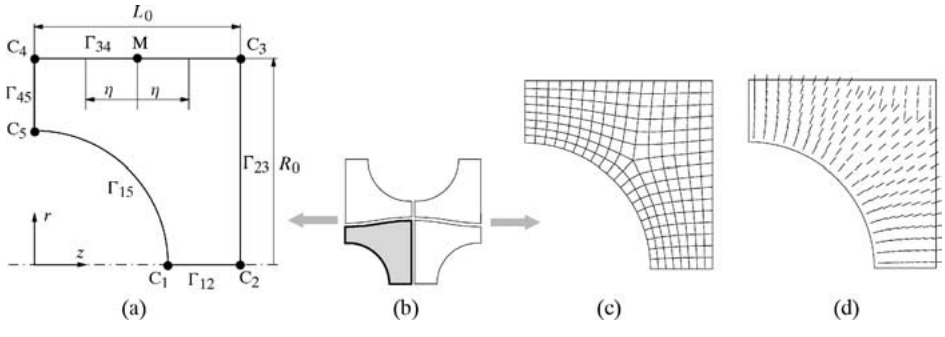

Figure 7 (a) Schematic visualization of an axisymmetric RVE model of a staggered array of particles, (b) neighboring RVEs in a deformed state, (c) finite element mesh, and (d) local material orientations.

coordinate:

$$[R_0 + u_r(z_0|_{\mathrm{M}} - \eta)]^2 + [R_0 + u_r(z_0|_{\mathrm{M}} + \eta)]^2 = 2[R_0 + u_r|_{\mathrm{M}}]^2. \quad (14)$$

Symmetry conditions along the right and left boundaries are written as

$$u_z|_{\Gamma_{23}} = u_z|_{\mathrm{C}_2}; \quad (15)$$

$$u_z|_{\Gamma_{45}} = u_z|_{\mathrm{C}_5}, \quad (16)$$

respectively. Since the axis of rotational symmetry coincides with boundary Γ_{12}, the following condition is imposed on this boundary:

$$u_r|_{\Gamma_{12}} = 0. \quad (17)$$

The axisymmetric RVE is subjected to tension at a macroscopically constant strain rate:

$$u_z|_{\mathrm{C}_2} - u_z|_{\mathrm{C}_5} = L_0[\exp(\dot{\varepsilon}t) - 1], \quad (18)$$

where the deformation rate $\dot{\varepsilon}$ is set equal to the material reference shear rate $\dot{\gamma}_0$.

The finite element mesh of the SA model, with 20 volume percent voids, is visualized in Fig. 7c. In each integration point of the 196 reduced integration 4-noded bilinear elements, a local coordinate system is generated, such that the local 1-directions are again perpendicular to the closest void surface, as is shown in Fig. 7d.

6. Effect of transcrystallized anisotropy on toughness

In this section, the full multiscale model will be used to investigate the effect of a transcrystallized orientation on the deformation of particle-modified systems. Both RVE models, as described in the previous section, are used, with in each integration point either an aggregate of randomly generated orientations or a (unique) set of orientations with a similar distribution as in Fig. 5. For the latter situation, the local (fiber) symmetry directions correspond to the 1-directions as described in Section 5.

In each integration point, 64 composite inclusions per aggregate are used.

In Fig. 8, for the plane strain ID model, the obtained fields of the magnitude of plastic deformation, $\bar{\varepsilon}_{\mathrm{p}}^{\mathrm{mag}} = \sqrt{\frac{2}{3}\bar{\varepsilon}_{\mathrm{p}} : \bar{\varepsilon}_{\mathrm{p}}}$, are shown for $\dot{\varepsilon}t = 0.025$. For the large scale RVE, containing randomly oriented, and thus quasi isotropic, matrix material, plastic deformation is localized in a particle-bridging path, percolating through the matrix, approximately perpendicular to the loading direction. The small scale RVE, having transcrystallized orientations, shows a more dispersed pattern of plastic deformation, with shear bands in relatively thick interparticle ligaments, in the 30° to 50° direction with respect to the particle poles (the term *pole* refers to the location where the particle/matrix interface normals are aligned with the loading direction). In the relatively thin ligaments, still localized deformation is observed. In Figs 9 and 10, the magnitude of plastic deformation is shown for $\dot{\varepsilon}t = 0.05$, as well as some selected microscopic texture evolutions and deformation quantities in two integration points, for random and transcrystallized initial orientations, respectively. For both situations, most plastic deformation is concentrated in relatively thin interparticle ligaments. The presence of a layer of preferentially crystallized material with significant thickness around cavitated rubber particles does have some effect on the mechanism of matrix shear yielding. This effect is however limited due to the limited level of anisotropy of the material.

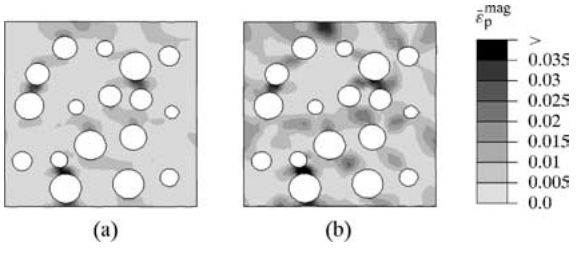

Figure 8 The influence of radially oriented anisotropy on the magnitude of plastic deformation, $\bar{\varepsilon}_{\mathrm{p}}^{\mathrm{mag}}$, for the ID model, at $\dot{\varepsilon}t = 0.025$, with (a) randomly generated initial orientations, and (b) transcrystallized preferential orientations.

In the pole figures showing the evolution of crystallographic and morphological texture, the initial orientation of each composite inclusion is represented by a dot. The arrow connects it with the corresponding final orientation, which is located at the arrow-head. In the pole figures showing microscopic deformation quantities, the location of each dot represents the initial orientation of the lamellar normal of an inclusion and its gray-value represents the value of the indicated quantity for the inclusion. The latter pole figures are enriched by reflecting each pole with respect to the central point of the plot. The view direction is the macroscopic out-of-plane direction. The term *intralamellar* deformation is employed for the magnitude of deformation of the crystalline phase and is represented for the ith inclusion by $(\varepsilon^{\mathrm{c}^i})^{\mathrm{mag}} = \sqrt{\frac{2}{3}\varepsilon^{\mathrm{c}^i} : \varepsilon^{\mathrm{c}^i}}$, with $\varepsilon^{\mathrm{c}^i} = \ln(\boldsymbol{U}^{\mathrm{c}^i})$. For the amorphous deformation, a distinction is made between so-called *interlamellar shear* and *interlamellar separation*. Let $\boldsymbol{y}^{\mathrm{a}^i}$ be a material vector in the amorphous phase of inclusion i, with $\boldsymbol{y}_0^{\mathrm{a}^i} = \boldsymbol{n}_0^{\mathrm{I}^i}$. Then, interlamellar shear is represented by the angle (in radians) between the convected material vector, $\boldsymbol{y}^{\mathrm{a}^i} = \boldsymbol{F}^{\mathrm{a}^i} \cdot \boldsymbol{n}_0^{\mathrm{I}^i}$, and the current lamellar normal, $\boldsymbol{n}^{\mathrm{I}^i}$. Lamellar separation is represented by $\ln(\lambda_{\mathrm{nn}}^{\mathrm{a}^i})$, with $\lambda_{\mathrm{nn}}^{\mathrm{a}^i} = \boldsymbol{n}^{\mathrm{I}^i} \cdot \boldsymbol{y}^{\mathrm{a}^i}$. Integration point A represents, for the initially randomly oriented material, a material point in the highly localized zone.

Since this integration point is located in the equatorial area (the *equator* is defined as the area where the particle/matrix interface normal is perpendicular to the loading direction), the local 1-direction is almost perpendicular to the global loading direction. The microscopic results for this point show moderate crystallographic deformation, mainly for inclusions with their lamellar normals close to the local 1-direction. The (100) poles, which represent the planes containing

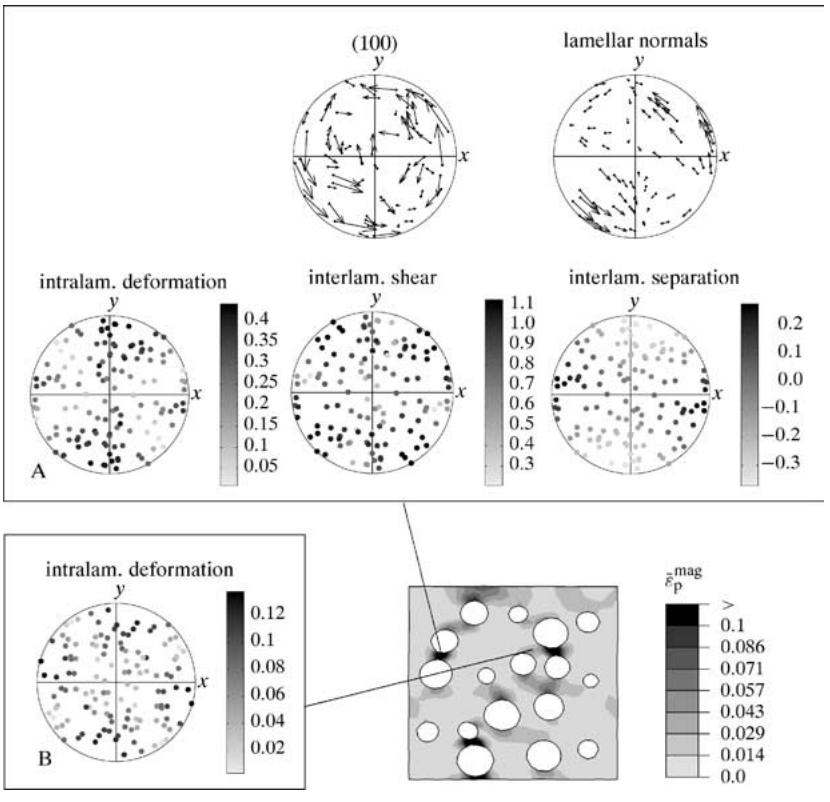

Figure 9 The magnitude of plastic deformation, $\bar{\varepsilon}_p^{mag}$, and selected microscopic results for the ID model, at $\dot{\varepsilon}t = 0.05$, with randomly generated initial orientations.

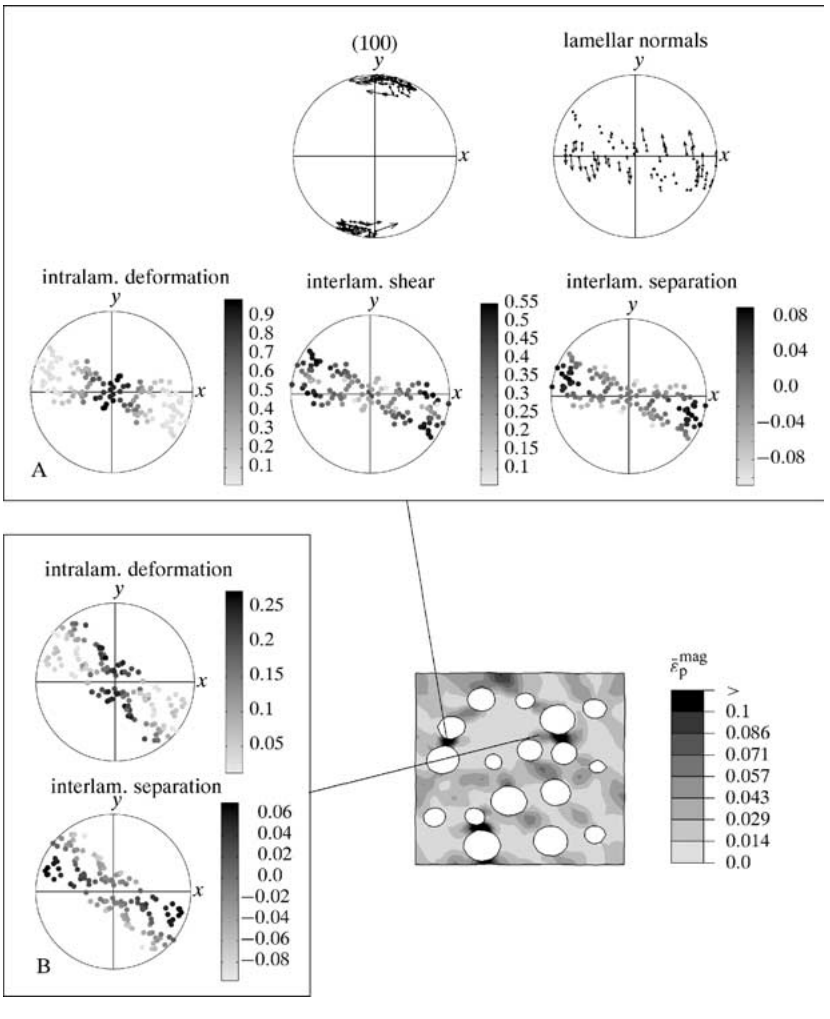

Figure 10 The magnitude of plastic deformation, $\bar{\varepsilon}_p^{mag}$, and selected microscropic results for the ID model, at $\dot{\varepsilon}t = 0.05$, with transcrystallized initial orientations.

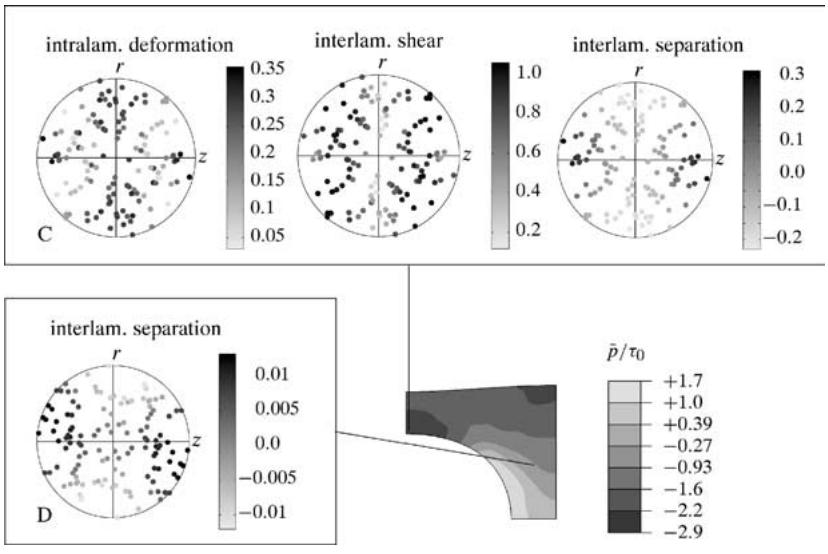

Figure 11 The normalized hydrostatic pressure, $\bar{p}/\tau_0$, and selected microscopic results for the SA model, at $\dot{\varepsilon}t = 0.1$, with randomly generated initial orientations.

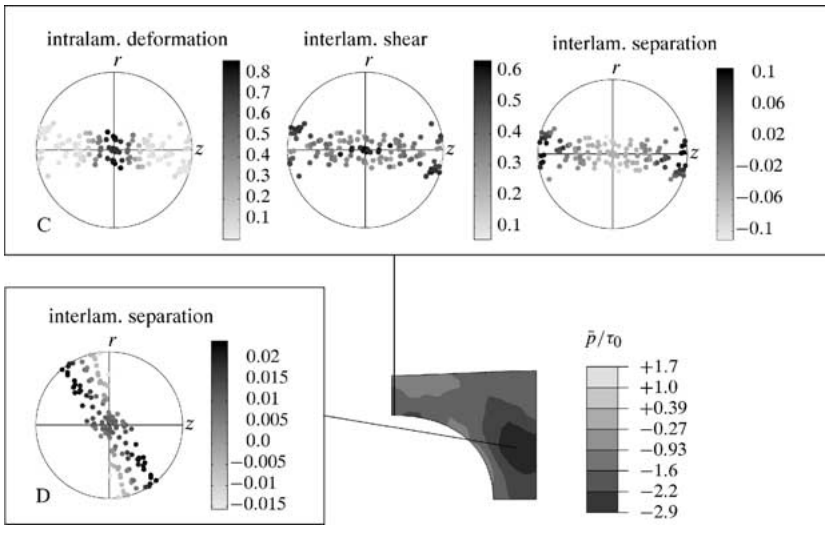

Figure 12 The normalized hydrostatic pressure, $\bar{p}/\tau_0$, and selected microscopic results for the SA model, at $\dot{\varepsilon}t = 0.1$, with transcrystallized initial orientations.

the two most easily activated slip systems, migrate towards a direction which is approximately 40° away from the local 1-direction. The lamellar normals are moving towards the same direction, with the largest activity for lamellar poles that are initially far from the target direction. Amorphous deformations are relatively large, with interlamellar shear predominantly in inclusions with their crystalline/amorphous interface approximately 45° inclined with the loading direction. Interlamellar separation is found predominantly in inclusions with their interface normals perpendicular to the local 1-direction. For the RVE with transcrystallized orientations (Fig. 10), deformation is still localized in the ligament containing integration point A. In this point, the maximum intralamellar (crystallographic) deformation has increased with respect to the quasi isotropic material, whereas both interlamellar shear and separation have decreased. Crystallographic deformation is concentrated in inclusions with their lamellar normals perpendicular to the loading direction. Also in integration point B, maximum intralamellar deformations are approximately doubled, whereas the magnitude of interlamellar deformations is comparable to the isotropic situation.

In Figs 11 and 12, the normalized hydrostatic pressure $\bar{p}/\tau_0$ is shown, as well as some selected microscopic texture evolutions and deformation quantities in two integration points, for the SA model, with random and transcrystallized initial orientations, respectively. The region of peak tensile triaxial stresses is located in the matrix material near the polar region for the preferentially oriented material, rather than in the equator region, as is observed for the randomly oriented material. In the equator region, the hydrostatic pressures remain negative; however the absolute values are reduced with respect to the quasi isotropic material. In Fig. 13, the direction and the magnitude of the normalized maximum in-plane principal stress, $\bar{\sigma}_{\max}/\tau_0$, are shown for the SA model. For the large scale, quasi isotropic material, the maximum principal stresses are found to be negligible in the polar region, whereas for the small scale configuration, with transcrystallized orientations,

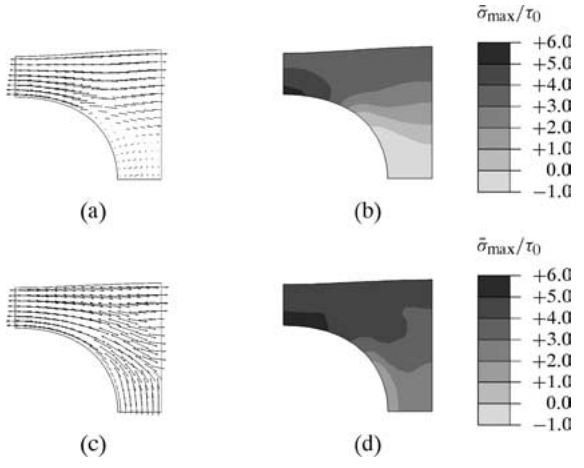

Figure 13 The direction and the magnitude of the normalized maximum in-plane principal stress, $\bar{\sigma}_{max}/\tau_0$, for the SA model, at $\dot{\varepsilon}t = 0.1$, with (a)–(b) randomly generated orientations, (c)–(d) transcrystallized preferential orientations.

also in this region, maximum principal stresses are significant. In the equator region, maximum values are slightly increased with respect to the principal stresses in the isotropic material.

For the initially randomly oriented configuration, in integration point C, which is located in the equatorial region, the intralamellar deformations are relatively small, and are found predominantly for inclusions with their lamellar normals either perpendicular or parallel to the loading direction. In the remaining inclusions, interlamellar shear is considerably large and a significant amount of interlamellar separation is found for inclusions with their lamellar normals aligned with the loading direction. For these inclusions, the preferred direction of craze growth, perpendicular to the direction of maximum principal stress, is parallel to the crystalline/amorphous interface. For the material with transcrystallized initial orientations, the maximum intralamellar deformations are more than doubled with respect to the randomly oriented material for inclusions with their lamellar normal perpendicular to the loading direction. Interlamellar deformations are considerably reduced. For integration point D, which is located in a high tensile triaxial stress area, lamellar separations remain small.

In polymeric materials, the principal mechanisms leading to deformation and fracture [34] are shear yielding of matrix material, voiding and the occurrence of crazelike features [35, 36] under triaxial stress conditions, and brittle fracture of the matrix by chain scission, induced by high tensile principal stresses. Whether or not the material will show toughened behavior will depend on which of these phenomena will predominantly occur. Massive shear yielding, with energy-absorbing inelastic deformation, will have a beneficial effect on toughening. However, for the transcrystallized orientation currently considered, the increase of matrix shear yielding (replacing strain localization) is limited. Intralamellar deformation is favored over interlamellar deformation. In the quasi isotropic material, crazelike features may be initiated in the equator region, where the peak tensile triaxial stresses are maximal, and significant interlamellar separation occurs. Since they will grow perpendicular to the direction of maximum principal stress, the growth direction will be transverse to the macroscopic tensile direction. These crazes may act as precursors to cracks, ultimately leading to failure. For the material having transcrystallized preferred orientations, in this region the negative hydrostatic pressures and interlamellar separation are reduced, diminishing the chance of craze initiation. On the other hand, in the polar region, for this material, relatively large tensile triaxial stresses are found, possibly initiating voids. However, interlamellar separation remains small at this location. In this area, the growth direction of possible crazes will be in the direction of macroscopic loading, and crazing may become an energy-absorbing mechanism. Therefore, transcrystallized orientations may lead to some degree of toughening, however the effect is limited by the relatively small amount of anisotropy.

7. Alternative microstructure

In the previous section, a fully radially oriented, transcrystallized, microstructure was shown to have a beneficial, but limited effect on the mechanics of deformation in particle-modified systems. This was attributed to the relatively small relative reduction in yield strength in the local 12 and 13 shear directions. A further decrease of these shear yield strengths would increase matrix shear yielding. Alternatively, an increase of the local 22 tensile yield strength, would have a similar effect, since it relatively reduces the strengths in shear.

A small flow-related crystallographic orientation was found by Bartczak *et al.* [11] in HDPE with calcium carbonate fillers. A row structure of polyethylene lamellae was found in extruded alternating high density polyethylene and polystyrene thin layers by Pan *et al.* [37]. The long axes of the lamellae, which are the crystallographic b-axes, were oriented in the plane of the layers and perpendicular to the extrusion direction. The a-directions were found to be predominantly normal to the layer surface and lamellar surface normals were aligned with the direction of flow. Moreover, only partial twisting was observed. In thicker layers, an unoriented structure was observed, similar to bulk polyethylene, with the corresponding lamellar twisting.

In this section, the effect of a hypothetical microstructure, with preferred orientations that may be the result of an influence of the process conditions on the crystallization of matrix material, will be investigated for a voided macrostructure. The transcrystallized preferred orientations as previously used, were axisymmetric with respect to the local 1-direction, i.e., within the plane of the particle/matrix interface, the orientation was assumed to be random. Here, an additional preferred orientation of the molecular chains and the lamellar normals in the local 2-direction is assumed. The thereby obtained lamellar row structure may be the result of an influence of the flow on the crystallization behavior, and resembles the structure that was reported by Pan *et al.* [37]. Again, the crystallographic {102} planes are assumed to form the crystalline/amorphous interface, with an initial tilt angle of 9.7°. In Fig. 14, a

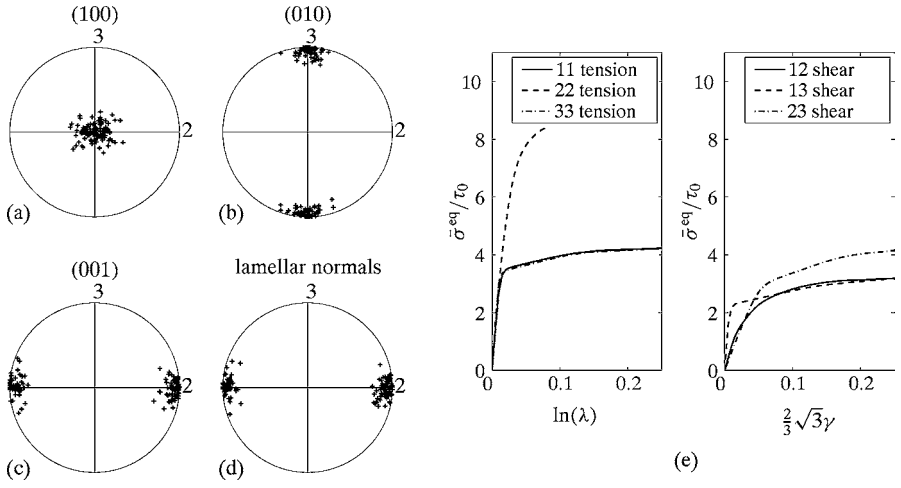

Figure 14 Equal area projection pole figures representing (a)–(c) the principal crystallographic lattice directions, and (d) the lamellar normals of an anisotropic set of orientations with an assumed influence of the flow and (e) the normalized equivalent mesoscopic stress $\bar{\sigma}^{eq}/\tau_0$, vs. the imposed deformation for tension and shear in the material base directions as predicted by the composite inclusion model.

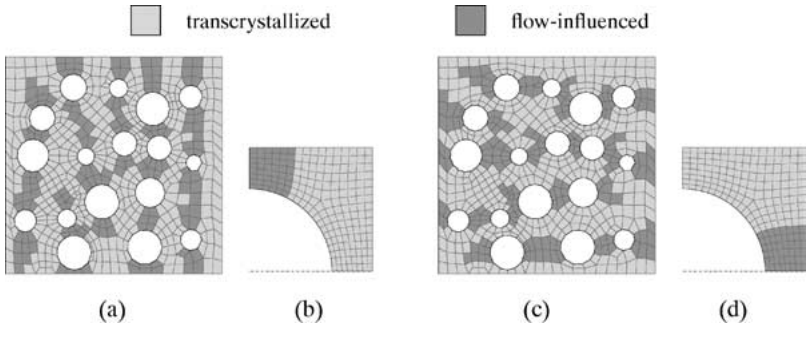

Figure 15 Assumed influence of flow on crystallization, with (a)–(b) flow in the loading direction and (c)–(d) flow perpendicular to the loading direction.

generated set of 125 composite inclusion orientations of this type are displayed. The obtained stress–strain behavior when this aggregate of composite inclusions is subjected to tension and shear in the basic material directions is shown in Fig. 14e. Because of the lack of a fiber symmetry in this material, large differences between the 22 and 33 tensile loading configurations are found. With respect to the transcrystallized orientations (Fig. 5), the yield strength in 22-direction has considerably increased, whereas the 33 yield strength is reduced. At $\ln(\lambda) = 0.05$ and $\frac{2}{3}\sqrt{3}\gamma = 0.05$, the ratio of the 22 tensile and 12 shear yield strength is 3.4. The ratio of the 22 tensile resistance and the 12 shear resistance of transcrystallized material is 3.0. When material with this microstructural morphology would, in a particle-dispersed system, be oriented appropriately with respect to the loading conditions, an additional beneficial effect on the amount of matrix shear yielding may be expected.

A microstructure of matrix material around well-dispersed voided particles is hypothesized that consists of lamellar crystals that are nucleated at the particle/matrix interface. An influence of processing conditions is assumed for matrix material in the equatorial regions (with respect to the flow direction). This hypothetical morphology is realized by assigning aggregates of composite inclusions with crystallographic and morphological orientations similar to the orientation set in Fig. 14 to specific elements of the finite element meshes which were previously used for the ID model and the SA model. These elements are located in the equatorial areas with respect to the flow direction. For the remaining elements, transcrystallized orientations are assumed (similar to Fig. 5). In Fig. 15, the flow-influenced areas are shown for both models, for either flow in the loading direction or flow perpendicular to the loading direction. In each integration point, the local 1-directions are assumed to be radially oriented with respect to the nearest particle, as was previously used for the transcrystallized situation. In Fig. 16, the effect of this microstructure on the obtained field of plastic deformation is shown for the ID model at $\dot{\varepsilon}t = 0.035$. In this figure, also the fully transcrystallized situation is represented. When the macroscopic loading is applied perpendicular to the flow direction, no significant effect of the flow-influenced orientations is observed, compared to fully transcrystallized material. However, when the RVE is loaded in the direction of the flow, plastic deformation is no longer localized in the relatively thin interparticle ligaments, but occurs predominantly in the matrix material, away from the particle surfaces and at the particle surface at an inclined location.

In Fig. 17a, the normalized hydrostatic pressure field is represented for the SA model, loaded in the flow direction. Results for the material loaded perpendicular to the flow direction are not shown because of the similarity with the fully transcrystallized situation. As

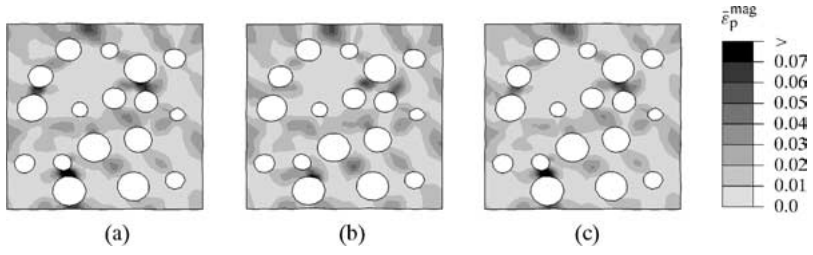

Figure 16 The influence of (a) transcrystallized orientations (b), (c) flow-influenced orientations on the magnitude of plastic deformation, $\bar{\varepsilon}_p^{mag}$, for the ID model, at $\dot{\varepsilon}t = 0.035$, with (b) flow in the loading direction, (c) flow perpendicular to the loading direction.

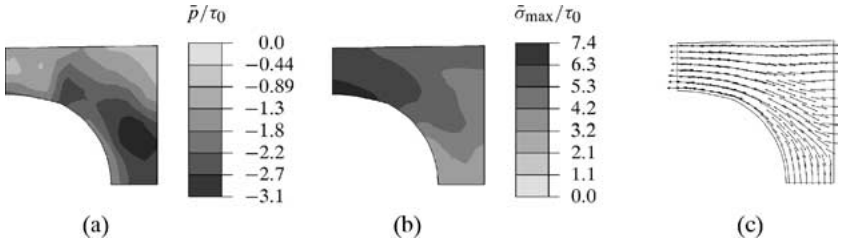

Figure 17 (a) The normalized hydrostatic pressure, $\bar{p}/\tau_0$ and (b), (c) the magnitude and the direction of the normalized maximum in-plane principal stress, $\bar{\sigma}_{max}/\tau_0$, for the SA model, at $\dot{\varepsilon}t = 0.075$, with the influence of flow in the loading direction.

for the fully transcrystallized situation, the area of peak tensile hydrostatic stress is relocated from the equatorial region for the quasi isotropic material to the matrix material near the particle pole. Fig. 17b and c show the normalized maximum in-plane principal stress for the SA model with the influence of flow in the loading direction. The largest maximum principal stresses are again observed in the equatorial area.

Thus, the hypothesized microstructure with local material orientations that may result from an influence of process conditions on crystallization may increase the toughening effects, if loaded in the appropriate direction with respect to the flow direction. Then, localization of deformation is replaced by dispersed shear yielding.

8. Conclusions

A physically-based mechanism for the toughening of semicrystalline polymeric materials by the dispersion of particles relies on the presence of a layer of anisotropic transcrystallized material around the particles [8, 10, 11]. In this work, a multiscale model was used to investigate the effect of such a preferentially oriented matrix material in HDPE blended with rubber particles, which were assumed to be cavitated. The particle-dispersed system was described by both an axisymmetric RVE model with an assumed regular stacking of voids and by a plane strain RVE model with irregularly dispersed voids, which were loaded in constant strain rate uniaxial tension. In each integration point of the finite element model, an aggregate of composite inclusions has been used as a representative microstructural element that provides the constitutive behavior of the material at the mesoscopic level. Constitutive properties were assigned at the microstructural level to both the amorphous and the crystalline phase. Besides these properties, the mesoscopic constitutive behavior was formed by the crystallographic and lamellar orientations of the composite inclusions. By using preferential initial orientations, a mesoscopically anisotropic constitutive behavior was obtained.

Simulations on voided polymeric material with a large average interparticle matrix ligament thickness, having quasi isotropic constitutive behavior at a mesoscopic level, showed a strongly localized deformation, forming a strain path through the matrix, perpendicular to the loading direction. Large tensile triaxial stresses were found in the equatorial region (with respect to the loading direction) near the particles. In this area, interlamellar separations were relatively large. A particle-modified system having a relatively small average interparticle matrix ligament thickness has been realized by using initially preferentially oriented lamellae, with the crystallographic (100) planes approximately parallel to the void/matrix interface. For this system, a more dispersed field of plastic deformation was found, induced by a small relative reduction of the shear yield strength. Moreover a relocation of the tensile triaxial stresses in the polar region, where deformation by interlamellar separation remains small, was observed, diminishing the likelihood of initiation and growth of crazelike features in the amorphous domains. These phenomena could indeed lead to some degree of toughening of the particle-modified material if the interparticle distance is small. However, with the level of anisotropy predicted by the composite inclusion model, the effects of these locally preferred orientations remain limited. Simulations on idealized polymeric material, modeled by anisotropic Hill plasticity, showed a much larger potential of local anisotropy for toughening of particle-dispersed semicrystalline materials, if the amount of anisotropy would be sufficiently large [13].

The level, and thereby the effect of local anisotropy was found to be improved if an additional hypothetical row structure of the transcrystallized lamellae was assumed in certain regions, which may be the result of processing conditions. When loaded in the direction of the macroscopic flow, plastic deformation was no longer localized in relatively thin interparticle

ligaments, but was largely dispersed through the matrix. This massive shear yielding, in combination with the effects on crazeinitiating conditions, will have a further beneficial effect on the behavior of this material, however only when loaded in the appropriate direction.

Acknowledgements

This research was funded through the Dutch Polymer Institute, project reference 163, "Deformation and fracture of polymer systems". The authors gratefully acknowledge Prof. D. M. Parks and Prof. M. C. Boyce of the Massachusetts Institute of Technology for their stimulating and helpful discussions concerning the modeling of particle-modified semicrystalline material.

References

1. S. WU, *Polymer* **26** (1985) 1855.
2. R. J. M. BORGGREVE, R. J. GAYMANS, J. SCHUIJER and J. F. INGEN HOUSZ, *ibid.* **28** (1987) 1489.
3. S. WU, *J. Appl. Polym. Sci.* **35** (1988) 549.
4. A. MARGOLINA and S. WU, *Polymer* **29** (1988) 2170.
5. T. FUKUI, Y. KIKUCHI and T. INOUE, *ibid.* **32** (1991) 2367.
6. K. DIJKSTRA and G. H. TEN BOLSCHER, *J. Mater. Sci.* **29** (1994) 4286.
7. O. K. MURATOĞLU, A. S. ARGON and R. E. COHEN, *Polymer* **36** (1995) 2143.
8. *Idem.*, *ibid.* **36** (1995) 921.
9. P. A. TZIKA, M. C. BOYCE and D. M. PARKS, *J. Mech. Phys. Solids* **48** (2000) 1893.
10. Z. BARTCZAK, A. S. ARGON, R. E. COHEN and M. WEINBERG, *Polymer* **40** (1999) 2331.
11. *Idem.*, *ibid.* **40** (1999) 2347.
12. B. A. G. SCHRAUWEN, L. E. GOVAERT, G. W. M. PETERS and H. E. H. MEIJER, *Macromol. Symp.* **185** (2002) 89.
13. J. A. W. VAN DOMMELEN, W. A. M. BREKELMANS and F. P. T. BAAIJENS, *Mech. Mater.* **35** (2003) 845.
14. *Idem.*, *Comp. Mater. Sci.* **27** (2003) 480.
15. J. A. W. VAN DOMMELEN, D. M. PARKS, M. C. BOYCE, W. A. M. BREKELMANS and F. P. T. BAAIJENS, *J. Mech. Phys. Solids* **51** (2003) 519.
16. C. G'SELL and A. DAHOUN, *Mater. Sci. Eng.* A **175** (1994) 183.
17. A. S. ARGON, *J. Comput. Aided Mater. Des.* **4** (1997) 75.
18. B. J. LEE, D. M. PARKS and S. AHZI, *J. Mech. Phys. Solids* **41** (1993) 1651.
19. E. M. ARRUDA and M. C. BOYCE, *ibid.* **41** (1993) 389.
20. D. C. BASSETT and A. M. HODGE, *Proc. Roy. Soc. London* A **377** (1981) 25.
21. D. C. BASSETT, A. M. HODGE and R. H. OLLEY, *ibid.* **377** (1981) 39.
22. Z. BARTCZAK, A. S. ARGON, R. E. COHEN and T. KOWALEWSKI, *Polymer* **40** (1999) 2367.
23. B. J. LEE, A. S. ARGON, D. M. PARKS, S. AHZI and Z. BARTCZAK, *ibid.* **34** (1993) 3555.
24. HKS. ABAQUS/Standard User's Manual, Version 6.2. Hibbitt, Karlsson & Sorensen, Inc., Pawtucket, Rhode Island, USA (2001).
25. J. A. W. VAN DOMMELEN, D. M. PARKS, M. C. BOYCE, W. A. M. BREKELMANS and F. P. T. BAAIJENS, in Proceedings of the European Conference on Computational Mechanics, Cracow, Poland, 2001.
26. A. KELLER and S. SAWADA, *Makromol. Chem.* **74** (1964) 190.
27. S. GAUTAM, S. BALIJEPALLI and G. C. RUTLEDGE, *Macromolecules* **33** (2000) 9136.
28. R. J. M. SMIT, W. A. M. BREKELMANS and H. E. H. MEIJER, *J. Mech. Phys. Solids* **47** (1999) 201.
29. S. SOCRATE and M. C. BOYCE, *ibid.* **48** (2000) 233.
30. R. J. M. SMIT, W. A. M. BREKELMANS and H. E. H. MEIJER, *Comput. Methods Appl. Mech. Eng.* **155** (1998) 181.
31. R. HALL, *J. Mater. Sci.* **26** (1991) 5631.
32. V. TVERGAARD, *J. Mech. Phys. Solids* **44** (1996) 1237.
33. *Idem.*, *Internat. J. Solids Struct.* **30** (1998) 3989.
34. H.-H. KAUSCH, R. GENSLER, CH. GREIN, C. J. G. PLUMMER and P. SCARAMUZZINO, *J. Macromol. Sci. Phys.* **B38** (1999) 803.
35. G. H. MICHLER and R. GODEHARDT, *Cryst. Res. Technol.* **35** (2000) 863.
36. I. NARISAWA and M. ISHIKAWA, Crazing in Semicrystalline Thermoplastics, Vol. 91/92 of *Adv. Polym. Sci.* (Springer-Verlag, Berlin, 1990) p. 353.
37. S. J. PAN, J. IM, M. J. HILL, A. KELLER, A. HILTNER and E. BAER, *J. Polym. Sci.*; *Part B*: *Polym. Phys.* **28** (1990) 1105.

Received 13 January
and accepted 29 July 2003